Recent progress on terahertz generation based on difference frequency generation: from power scaling to compact and portable sources

(Invited Paper)

Yujie J. Ding[1*], Pu Zhao[1], Srinivasa Ragam[1], Da Li[1], and Ioulia B. Zotova[2]

[1] *Department of Electrical and Computer Engineering, Lehigh University, Bethlehem, PA 18015, USA*

[2] *ArkLight, P. O. Box 2, Center Valley, PA 18034, USA*

[*] *Corresponding author: yud2@lehigh.edu*

Received July 18, 2011; accepted August 3, 2011; posted online September 30, 2011

The progress achieved on power scaling and compact and portable THz sources is reviewed. By reversely stacking the GaP plates, the photon conversion efficiency is improved from 25% to 40% which corresponds to the maximum value. When the number of the plates is increased from four to five, the output power decreases because of back conversion. The THz generation is also investigated by mixing the two frequencies generated by a single Nd:YLF solid-state laser. The average output power reaches 1 μW. The introduction of two Nd:YLF crystals significantly improves the output power to 4.5 μW. This configuration facilitates the generation of different output frequencies.

OCIS codes: 190.4410, 190.4360, 190.4975, 140.3540, 140.3580.

doi: 10.3788/COL201109.110004.

1. Introduction

We adhere to several major reasons for taking advantage of the terahertz (THz) region of the electromagnetic spectrum with the corresponding frequencies between 0.1 THz and 10 THz. Firstly, the transition frequencies between the rotational states in gases typically exist in this region[1]. Therefore, one can develop a relatively compact spectrometer to fingerprint molecules. Since the linewidth for the rotational transitions can be 50 MHz (0.0017 cm^{-1}) or narrower for low-pressure gases, the spectrometer must have a sufficiently high resolution to resolve each rotational transition. In comparison, most molecules exhibit the congested and unresolved ro-vibrational spectra in the visible to mid-infrared domains[2]. Therefore, it may not be feasible to fingerprint correctly the molecules in these domains. Secondly, the identification and detection of biological agents based on the THz spectroscopy have become increasingly important[3]. Thirdly, owing to the presence of atmospheric windows, THz waves can be used for probing as well as imaging[4]. Based on the discussion above, it is important to develop a THz system that is capable of taking the multi-spectral images of targets and simultaneously analyzing the targets based on the THz spectra measured by a tunable and monochromatic THz source.

Broadband THz pulses are generated based on optical rectifications[5], photoconduction[6], and Cherenkov radiation[7]. These schemes require ultrafast laser pulses. To sense chemicals, time-domain spectroscopy has been developed[8]. These broadband pulses are used to measure rotational spectra of gases[9], identify explosives[10], and obtain THz images[11].

Aside from optical rectifications, other parametric processes in nonlinear crystals can be relatively efficient in converting optical pulses into THz waves. For example, based on the THz parametric oscillation in a $LiNbO_3$ crystal[12], the output power on the level of ~mW has been generated in the range of 140−290 μm (1.03−2.14 THz). By mixing two coherent infrared laser beams in nonlinear-optical crystals such as GaSe[13−15], $ZnGeP_2$[16−18], and GaP[19,20], the THz waves have been efficiently generated with extremely-wide tuning ranges and very high peak powers as well as high conversion efficiencies. In the present work, the widest tuning range achieved covers the wavelengths within the range of 66.5 μm to 5.66 mm (from 4.51 THz down to 53 GHz) based on the type-*oe*-*e* phase-matched difference frequency generation (DFG). On the high-frequency side of the reststrahlen band, we generated the radiation that is tunable in the range of 2.7−28.7 μm using a different phase-matching configuration[21]. The tuning range achieved almost covers the entire THz region (0.1−10 THz) and a part of the millimeter-wave or microwave domain, i.e., 1 mm to 5.66 mm (53−300 GHz). The highest output peak powers measured are 389 W at 203 μm (1.48 THz) and 4.7 W at the wavelength of 1 mm (300 GHz), corresponding to the conversion efficiencies of 0.098% and 0.0012%, respectively, in terms of the pulse energies. The highest photon conversion efficiency is approximately 19%[15].

Several important applications were explored using our widely-tunable THz sources. By measuring the absorption spectra of the commonly-used chemicals in the vapor phase, we demonstrated that the developed THz absorption spectrometer can be used to fingerprint a class of molecular species[22,23]. The transmission spectra of the isotopic variants[23,24], biological species[14,25], and VX nerve agent[26] can be measured as well.

Recently, the photon conversion efficiency has been improved from 25%[27] to 40% by reversely stacking GaP plates[28]. We demonstrated that 40% corresponds to

the maximum conversion efficiency[28]. As the number of the stacked GaP plates was increased from four to five, the output power decreased due to back conversion. To make our THz source truly compact and portable, we investigated the THz generation by mixing two frequencies generated by a single Nd:YLF solid-state laser[29]. The average output power reaches 1 μW at 1.64 THz[29]. This THz source can have the dimensions of 12×12×6 (inch). By introducing two Nd:YLF crystals in the laser cavity, the output power is significantly improved to 4.5 μW[30]. Such configuration allowed us to generate different THz frequencies by combining two different laser crystals[30]. Through further optimizations and utilization of novel configurations, the dimensions of the THz source may be reduced to 12×6×4 (inch) and eventually to the size of a laser pointer.

In the current work, we review our past efforts on the power scaling of the THz waves generated by mixing two near-infrared coherent radiation beams in stacked GaP plates. We also summarize the recent results on the development of compact and portable THz sources by mixing a pair of frequencies generated by dual-frequency solid-state lasers.

2. Power scaling by stacking GaP plates

In this section, we summarize our results on the power scaling of the THz radiation based on DFG in high-resistivity and low-dislocation-density GaP plates[27]. The GaP plates were stacked in a manner wherein the three non-zero elements of the second-order nonlinear susceptibility have the same sign or opposite signs from one plate to the next. These two stacking configurations yielded completely different results in terms of the highest output peaks and corresponding wavelengths. The highest output peak power was approximately 2.36 kW, which is two orders of magnitude higher than our previous result[19,20].

Each of the semi-insulating undoped (110) GaP plate used in the experiment has a resistivity of $>$ 1.0 MΩ-cm and a dislocation density of 2.25×10^5 cm^{-2}. Each GaP plate has a diameter of 48.5 mm and a thickness of 663 μm. Both of the (110) facets are polished. To generate monochromatic THz pulses, two coherent radiation beams were used. These are the Nd:YAG laser at 1.064 μm with pulse duration of 10 ns and a pulse energy of 20.7 mJ (the highest pulse energy used in our experiment) and the idler output from a β-BaB_2O_4-based optical parametric oscillator (OPO) pumped by the third-harmonic output of the Nd:YAG laser. The highest pulse energy for the idler beam is 18.7 mJ with a pulse duration of 5 ns. These two beams were collimated and combined. Subsequently, the GaP plates were illuminated. The beam radius for both of the mixing beams at the GaP plates was measured to be 1.0 mm. Therefore, the highest peak intensity for the idler beam was 120 MW/cm^2, which is a factor of 5.4 below the 650 MW/cm^2; the highest intensity used which did not cause any damage[31]. They propagated collinearly in a direction perpendicular to the two large facets of the GaP plates with their polarizations parallel to the [1,−1,0] and [0,0,1] directions. Under such configuration, the effective second-order nonlinear coefficient is significantly higher than that from a (100) GaP crystal[19,20]. Germanium and polyethylene windows were used to block the two mixing beams. The THz radiation generated by DFG was attenuated and collimated by a parabolic mirror, and subsequently focused onto a power meter using another parabolic mirror. The THz output wavelengths were calibrated by an etalon.

The absorption spectrum was deduced by measuring the transmission and reflection spectra of each GaP plate using Fourier transform infrared spectroscopy. Figure 1 shows that the absorption coefficient is 2.2 cm^{-1} at 120 μm, which is 7 times lower than the absorption coefficient from our previous sample. This implies that a maximum of seven plates can be stacked to increase the output power effectively. Based on the dispersion relation available[32], the coherence length for the THz generation was linearly increased with the wavelength from 581 μm at 76.5 μm. At 304 μm, the coherence length becomes 7.37 mm. The THz output powers were measured at different output wavelengths. Figure 2 shows that the THz output radiation is tuned continuously from 3.91 THz (76.7 μm) to 454.9 GHz (659.5 μm). The tuning range was achieved by slightly adjusting the frequency (wavelength) of the idler beam generated by the OPO. Within this range, the plate thickness is either

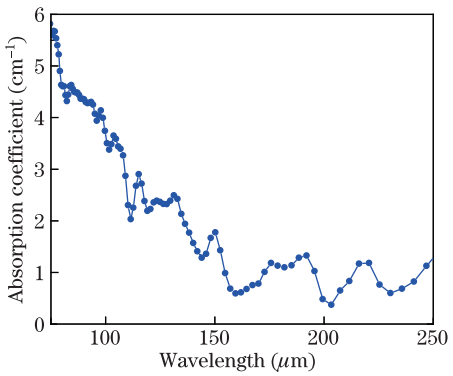

Fig. 1. Absorption coefficient as plotted against the wavelength, following the measurement of transmission and reflection spectra on a single GaP plate.

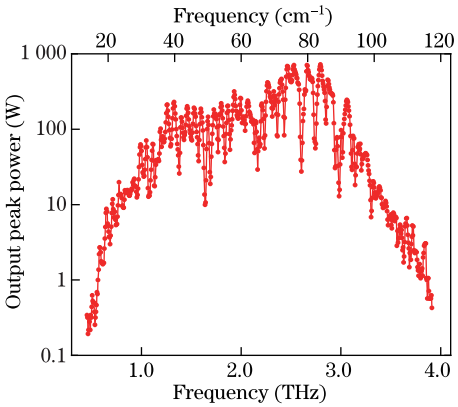

Fig. 2. THz output power as measured against the output wavelength for a single GaP plate. As discussed in the text, the modulations are caused by convolution between the Fabry-Perot effect for THz wave and water-vapor absorption.

comparable to or shorter than the coherence length that we have calculated. Therefore, the THz generation is phase-matched. At 2.775 THz (108.1 μm), the output power reached the highest value, i.e., 722 W. Using the pulse width of ~5 ns, the highest average power of the generated THz radiation is 36.1 μW under the average input power of 207 mW at 1.0642 μm and 187 mW at 1.0748 μm. This output power is a factor of 46 larger than the highest peak power achieved on GaP so far[19,20].

Using a (110) GaP wafer, a considerably higher value of the effective second-order nonlinear coefficient can be accessed[20]. Second, the two parallel facets of the GaP crystal can induce the Fabry-Perot effect which can also contribute to the enhancement of the THz output power. As shown in Fig. 2, the THz output power changes periodically. On the low-frequency side, i.e., for the frequencies below 2.5 THz, the frequencies at most of the peaks and valleys can match the frequencies calculated based on the Fabry-Perot effect. If we only assume such effect for the THz wave, the ratio of a local maximum power and its adjacent minimum value should be approximately 3.3. For frequencies higher than 2.5 THz, the frequencies at the peaks and valleys have become inconsistent with those predicted by the Fabry-Perot effect. In addition, the modulation depths are larger. We believe that these modulations are primarily caused by the water vapor absorption. Third, the absorption of the THz pulses generated by the DFG is less than that of the previous crystal[19,20]. As a result, the frequency at the highest output power from our crystal (2.775 THz) is higher than the frequency previously measured, i.e., 1.73 THz[19,20]. Subsequent absorption of the THz pulses by a relatively thick crystal occurs at relatively high frequencies[19,20]. This assumption is further supported by the fact that the high-frequency limit measured on our crystal is significantly higher than the previous value. Fourth, given that the dislocation density of the GaP crystal is remarkably low, the damage threshold is significantly increased. As a result, we were able to use higher peak powers for the two mixing beams.

The dependence of the THz output power on the input power of one of the mixing beams was measured. Based on the linear least square fitting of the power dependences, we determined that the internal conversion efficiency is 0.067% (the photon conversion efficiency is 6.8%). Without taking into consideration the absorption losses, and by considering the Fabry-Perot effect for the THz wave while assuming that the three non-zero elements of the second-order nonlinear optical susceptibility for GaP are identical, the maximum conversion efficiency for the THz generation in terms of peak powers can be given by[33]

$$\eta_{\max} = \frac{P_{\mathrm{THz}} T_{\mathrm{THz}}^{-1}}{P_1 T_1} = \frac{16 d_{\mathrm{eff}}^2 L^2}{\varepsilon_0 c n_1 n_2 n_{\mathrm{THz}} \lambda_{\mathrm{THz}}^2} \frac{P_2}{\pi w_0^2} \frac{T_2}{T_{\mathrm{THz}}^2}, \quad (1)$$

where max is used to designate the local maximum values as a result of the Fabry-Perot effect; d_{eff} is the effective nonlinear coefficient; P_{THz} is the THz output peak power; P_1 and P_2 are the input peak powers at 1.064 μm and at the idler wavelength, respectively; λ_{THz} is the output wavelength; L is the total thickness of the GaP wafer; w_0 is the beam radius for the pump beams; n_i (i=1,2) represents the refractive indices of the GaP crystal at the respective wavelengths of the three interacting waves; and T_i (i=1,2) is the Fresnel transmission coefficients at single surface. Assuming that $d_{\mathrm{eff}} \approx 47$ pm/V, $\eta_{\max} \approx 0.015\%$ is obtained from Eq. (1). This value is approximately a factor of 4.5 lower than our experimental value. We believe that the difference between the two may have been caused by the uncertainty of the value of d_{eff} used in Eq. (1).

In addition to one GaP plate, we attempted to stack two and three GaP plates. The GaP plates were stacked according to two different configurations, i.e., the three elements of the second-order nonlinear susceptibility for GaP have (A) the same sign and (B) opposite signs between the adjacent GaP plates. Figure 3 illustrates the result obtained for the stacking configuration A. The wavelength corresponding to the highest output power has been significantly red-shifted from 108.1 to 204.8 μm and to 303.9 μm. The corresponding power is reduced from 722 to 698 W and subsequently to 611 W. The 611 W value corresponds to a photon conversion efficiency of 16% inside the stacked plates. These results indicate the existence of an optimal interaction length for each specific output wavelength. We believe that the red-shift of the optimal output wavelength is primarily due to the combination of the linear wavelength dependence of the coherence length and wavelength-dependent output power reflected by Eq. (1). Therefore, at the wavelengths of 108.1 μm, 204.8 μm, and 303.9 μm, the coherence lengths must be approximately close to 663 μm, 1.326 mm, and 1.989 mm, respectively.

Under the stacking configuration B, the result is completely different. Figure 4 shows that the wavelength corresponding to the highest output power is maintained at 120.3 μm for the two and three plates. Therefore, quasi-phase matching is achieved at this wavelength. This implies that the coherence length at 120.3 μm is approximately 663 μm. On the other hand, using the dispersion relation[32], the coherence length is 1.65 mm. We believe that the factor of 2.5 between the two is probably a result of the inaccuracy in the THz index of refraction calculated using the dispersion relation[32]. Using 663 μm as the coherence length, we determined that the

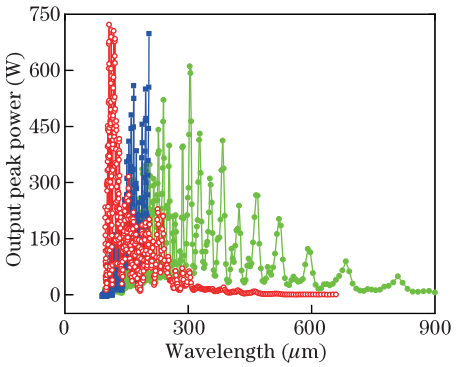

Fig. 3. Output peak power versus the wavelength: single GaP plate (open circles); stacked two GaP plates (squares); stacked three GaP plates (dots). For both the stacked two and three plates, the second-order nonlinear coefficients have the same sign between the adjacent plates.

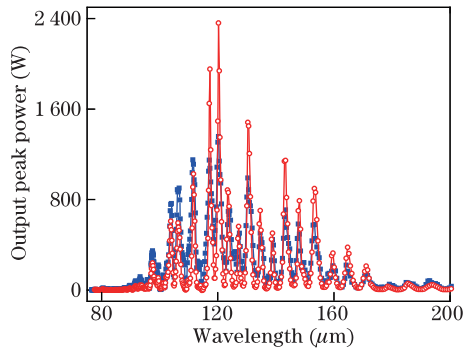

Fig. 4. Output peak power versus the wavelength: stacked two GaP plates (squares); stacked three GaP plates (open circles). For both the stacked two and three plates, the second-order nonlinear coefficients have the opposite signs between the adjacent plates.

index of the refraction at 120.3 μm is 3.217. This is 3.8% lower than the value derived in Ref. [32]. The estimate illustrates that the coherence length is relatively sensitive to the index of the refraction at the output wavelength. In this wavelength, the output peak power significantly increased from 433 W to 1.36 kW and 2.36 kW, corresponding to two and three plates, respectively. The peak power of 2.36 kW corresponds to an average power of 118 μW. Compared with our previous results[19,20], the peak power increased by a factor of 151, i.e., two orders of magnitude. The internal conversion efficiency deduced from our experiment is 0.22%, which corresponds to the photon conversion efficiency of 25%.

3. Saturation of conversion efficiency and back conversion

In this section, we summarize our results of previous investigations on the power scaling of the THz generation based on DFG by stacking the GaP plates[28]. In particular, the maximum photon conversion efficiency of 40% was achieved. The THz peak power generated reached 4 kW. As the number of the GaP plates is increased from four to five, the output power decreased because of back conversion.

Similar to the section above, two coherent input beams were mixed in the stacked GaP plates. The first beam has the highest input peak power of 1.5 MW at 1.064 μm (10 ns; 10 Hz). The second beam generates an output wavelength tunable in 1.079−1.066 μm (5 ns; 10 Hz) with the highest peak power of 4.1 MW. The two collimated beams were directed to the GaP plates without focusing (the beam radii of 1 mm). The total intensity of the two beams at the GaP plates is 178 MW/cm^2. Each GaP plate has a diameter of 48.5 mm and a thickness of 663 μm. They were cut and polished along the (110) plane and stacked between a pair of aluminum plates. The two input beams propagated along the [110] direction with their polarizations parallel to [1−10] and [001]. The output THz radiation was attenuated by filters and subsequently measured using a power meter.

To achieve quasi-phase matching (QPM) for the THz generation, every other plate was rotated by 180°. That procedure is named as the alternatively-rotated stacked GaP plates (i.e., reversed plates). In this case, the second-order nonlinear coefficient changes its sign between any adjacent ones. To find out the enhancement factor caused by the QPM, we compared the first stacking configuration with the second stacking configuration in which all the GaP plates are perfectly aligned such that their respective crystalline axes are all in the same directions (i.e., aligned plates). Therefore, the second-order nonlinear coefficients of all the plates have the same sign.

The spectrum of the THz output generated by the four reversed plates (with total thickness of 2.65 mm) was measured. As illustrated by Fig. 5, the generated THz radiation is continuously tuned from 78 to 300 μm. The highest output peak power is 2.73 kW (the corresponding power of 3.77 kW generated inside the plates) under the input powers of 1.5 MW and 4.1 MW at 1.064 μm and 1.074 μm, respectively. At these powers, the output wavelength is 120.3 μm, which is chosen as a compromise between the THz absorption dictating the effective interaction length and the dependence of the optimal power on the THz wavelength, as shown in Eq. (3). The corresponding power conversion efficiency, defined as $P_{\rm T}/P_1$, where $P_{\rm T}$ and P_1 are the THz peak power and input peak power at 1.064 μm, was determined to be 0.182%. Taking into consideration the Fresnel reflections for the input beam at the entrance facet and THz output radiation at the exit facet, we obtained the internal photon conversion efficiency of 39.6%. The optimal THz output wavelength of 120.3 μm corresponds to the first-order QPM condition in the GaP plates having a period of 1.326 mm for the spatially modulated second-order nonlinear coefficients. The modulations in Fig. 5 including those in the 120−160 μm range are due to the water-vapor absorption and Fabry-Pèrot effect in the GaP parallel plate.

The spectrum of the THz output radiation generated by four aligned plates was measured. Figure 6 shows the generated THz radiation which covers the range of 135−500 μm. Below 135 μm, the output powers were relatively low because of the nearly zero values of the sine function (Eq. (2)). The highest output power reached 510 W at the wavelength of 236 μm under the input power of 4.1 MW at 1.069 μm. The power conversion efficiency is 0.034%. The corresponding internal photon conversion efficiency is 14.6%, which is significantly lower than the photon conversion efficiency for the

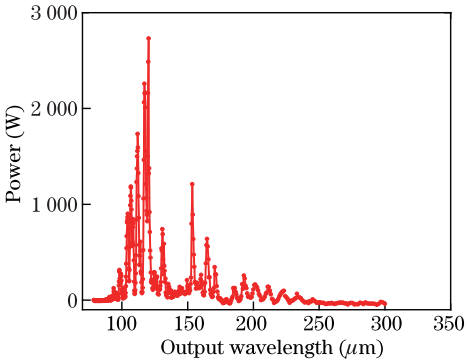

Fig. 5. Spectra of the THz output generated by the four reversed GaP plates, covering a range of 78−300 μm.

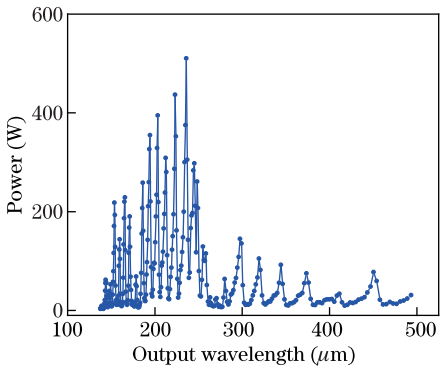

Fig. 6. Spectra of the THz output generated by the aligned four GaP plates, covering a tuning range of 135−500 μm.

reversed GaP plates. Based on this value, the optimal THz wavelength is primarily determined by the combination of the absorption and inverse-wavelength dependence of the THz power (Eq. (1)). Even though the aligned plates can be used to achieve phase-matching at sufficiently long THz wavelengths, the inverse dependence and increased optimal power (Eq. (3)), can make the reversed plates outperform the aligned plates significantly.

Figure 7 shows the dependence of the internal photon conversion efficiency on the average input power. For the four reversed plates, the conversion efficiency increased linearly below the average power of 50 mW for the input beam at 1.074 μm. However, as the average power increased further, the saturation of the conversion efficiency becomes obvious. When the input power approaches 200 mW, the conversion efficiency reaches a maximum value. The highest conversion efficiency achieved in our experiment is 39.6% at the input power of 204 mW. Considering the repetition rate of 10 Hz, pulse width of 5 ns, and beam size of 1 mm, this high conversion efficiency was achieved at pump intensity of 130 MW/cm^2 at 1.074 μm. Assuming $P_2 >> P_1$, where P_2 is the peak power at 1.074 μm, the photon conversion efficiency for the THz generation inside the GaP plates can be obtained as[34]

$$\eta_{\rm p} = \eta_{\rm max} \sin^2 \left[(\pi/2) \sqrt{P_{\rm ave}/P_{\rm opt}} \right], \qquad (2)$$

where $\eta_{\rm max} = a_{\rm T}/a_1$ is the maximum conversion efficiency with $a_{\rm T}$ and a_1 being the areas of the THz radiation and input beam at 1.064 μm, and $P_{\rm ave}$ is the average input power at 1.074 μm. In Eq. (1), the optimal power $P_{\rm opt}$ is obtained as

$$P_{\rm opt} = \frac{c\varepsilon_0 n_1 n_2 n_{\rm T} \lambda_1 \lambda_{\rm T} a_2 \tau_2 R}{16 d_{\rm eff}^2 L^2 T_2}, \qquad (3)$$

where $d_{\rm eff}$ is the effective second-order nonlinear coefficient; a_2, τ_2, and T_2 are the beam area, pulse duration, and transmittance at 1.074 μm, respectively; and R is the repetition rate. Following the nonlinear least-square-fit to the data points in Fig. 7 using the Eq. (2), we obtained $\eta_{\rm max} \approx 40.0\%$ and $P_{\rm opt} \approx 209$ mW. Therefore, the maximum photon conversion efficiency has been achieved in our experiment. To the best of our knowledge, this was the first report on the complete saturation of the conversion efficiency for the THz pulses generated by DFG[28]. Based on $\eta_{\rm max} \approx 40.0\%$, we obtained $a_{\rm T} \approx 0.400\ a_1$. Let us assume that the two input beams have Gaussian spatial distributions with exactly the same beam sizes, i.e., $a_1 = a_2$. After neglecting the effect of the saturation of the conversion efficiency, $a_{\rm T} \approx 0.5\ a_1$ was obtained. The deviation of our result from theory is attributed to the smaller effective area for the input beam at 1.074 μm. In addition, the weak reflections among the adjacent GaP plates could have contributed to the deviation. In comparison, no obvious saturation was observed on the aligned plates, (Fig. 7). The highest photon conversion efficiency is 14.6%. If this value is significantly increased, more complicated expression has to be introduced by taking into the consideration the phase-mismatch factor[34] to fit the saturation behavior.

With the increase in the number of the GaP plates from four to five, the THz output peak power significantly decreased from 2.73 kW for the four plates to 2 kW for the five plates (Fig. 8). The decrease in the THz output peak power is due to the back parametric conversion. Because the optimal power is inversely proportional to the square of the length, i.e., L^{-2}, (Eq. (3)), Eq. (2) was used to achieve a good fit of the data points in Fig. 8. Using thicker GaP plates, the QPM wavelength can be increased such that a larger number of the plates may be stacked to reach the zero output power beyond the optimal point, as shown in Fig. 8 and predicted by Eq. (2).

4. Compact and portable THz source

In this section, we summarize our previous results following the demonstration of a compact and portable THz source implemented based on DFG in a GaSe crystal[29]. An average THz output power can be as high as 1 μW at 1.64 THz (182 μm) in a linewidth of 65 GHz, corresponding to the peak power of 20 mW.

In our experiment, a Nd:YLF crystal was chosen as the lasing medium; aware that the two different frequencies of 286.5 THz and 284.9 THz (wavelengths of 1 047 nm and 1 053 nm) can be generated from a single Nd:YLF laser. Nd:YLF crystal is birefringent and thus, it emits two transitions at 1 047 nm and 1 053 nm with polarizations orthogonal to each other, designated by π

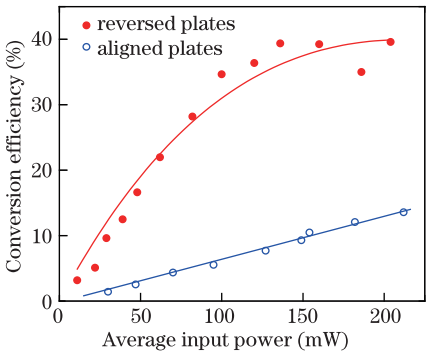

Fig. 7. Conversion efficiency for the THz generation versus the input power at 1.074 μm for the four reversed GaP plates (dots) and 1.069 μm for the four aligned GaP plates (circles). The straight line (bottom) represents the linear fit, whereas the curve (top) is fitted using Eq. (2).

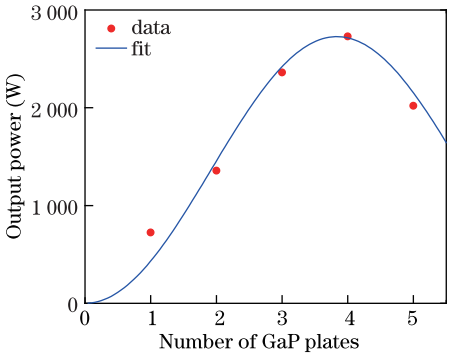

Fig. 8. Highest THz output power generated by the reversed GaP plates versus the number of plates. The curve represents the nonlinear least squares fit to the data points using Eq. (2).

and σ, respectively. The two transitions have the stimulated emission cross sections of 1.8×10^{-19} cm^{-2} and 1.2×10^{-19} cm^{-2} at 1 047 nm and 1 053 nm, respectively. Thus, it is feasible to tailor the output powers at these two wavelengths from a single laser crystal to be close to each other. In this case, the corresponding THz power reaches an optimal value under the same sum of the two input powers. Moreover, the THz output frequency generated by mixing these two laser beams is 1.643 THz (i.e., the wavelength of 182.42 μm), which is sufficiently close to 200 μm. Therefore, the THz output power is close to the maximum value obtained from a GaSe crystal[13−15]. Furthermore, a Nd:YLF crystal is known for its low thermal effect and long upper-state lifetime. In the past, a single Nd:YLF crystal has been used to simultaneously generate the output beams at 1 047 nm and 1 053 nm without introducing any optical element inside the single laser resonator[35]. However, the ratio of the powers generated at these two wavelengths cannot be controlled. In addition, the laser output powers are too low for the efficient generation of a THz output based on DFG. Although a Q-switched Nd:YLF laser has been implemented at 1 053 nm[36], the simultaneous lasing of the two wavelengths has not been achieved. Aside from the Nd:YLF crystal, other combinations of the active ions and host materials can also emit two different frequencies[37]. The Q-switched solid-state lasers may be one of the optimal choices for implementing a compact THz source based on DFG.

Figure 9 shows the experimental setup. The section bordered by a closed-loop dashed line is the schematic for a dual-frequency Nd:YLF laser. In principle, the coherent beams can be simultaneously generated at 1 047 nm and 1 053 nm from a single Nd:YLF laser. However, under this condition, balancing the output powers at the two wavelengths cannot be achieved because of the strong competition between the gains for the two transitions within the same laser medium. In our experiment, an intracavity polarizer was introduced to separate the two perpendicularly polarized beams into two laser cavities, both of which share the same lasing medium to alleviate the gain competition. In our design, the input mirror (IM), output couplers (OC1), and polarizer (P) are the components of the cavity for lasing at 1 047 nm (π, o-wave), whereas IM, P, and couplers OC2 compose the cavity for lasing at 1 053 nm (σ, e-wave). An a-cut 1.0% Nd-doped YLF (4×4×10 mm) crystal is shared in one arm by the two laser cavities. A plano input mirror (IM) was coated to facilitate the simultaneous production of high transmittance of $T > 95\%$ at 808 nm and high reflectivities of $R > 99.5\%$ at 1 047 nm and 1 053 nm. The polarizer P was coated in such a manner that when it is placed at a Brewster's angle relative to the input beam, the π-polarized beam has a high transmittance of $T \approx 98\%$, whereas the σ-polarized beam has the high reflectivity of $R > 99.9$. The Nd:YLF crystal was pumped by a diode laser through a fiber pigtail after the laser beam was collimated by a lens assembly. The diode laser dimensions of 1.75×1.25 (inch) allowed portability. Considering that the stimulated emission cross section for the 1 047 nm transition is 50% larger, one of the most effective approaches for balancing the output powers of the two transitions is to introduce an additional amount of cavity loss for the 1 047 nm beam. First, we have specifically chosen the different reflectivities for the two output coupler, which are 75% and 80% at 1 047 nm (OC1) and 1 053 nm, respectively. As a result, the lasing thresholds for the two transitions become closer to each other. Second, the output coupler (OC1) was slightly tilted to introduce an additional amount of the loss at 1 047 nm. To generate the high peak powers sufficiently, an acoustic-optic Q-switch was placed next to the Nd:YLF crystal in such a way that it is shared by the two beams oscillating in the two cavities. This represents an important method for the synchronization of the output pulses generated from the two laser cavities. The typical dimensions of the entire THz source, as illustrated in Fig. 9, are approximately 12×12× 6 (inch). Through further optimization, the dimensions can be reduced to 12×6×4 (inch). In addition, the compact THz source consumes $\leqslant$ 20 W. Therefore, it can be readily packaged into a portable system for field applications.

Figure 10 shows the dependence of the Q-switched output powers at 1 047 nm and 1 053 nm as well as the sum of the output powers from the laser diode. Based on the measurements, the lasing thresholds are 1.17 W and 1.64 W at 1 047 nm and 1 053 nm, respectively. Figure 10

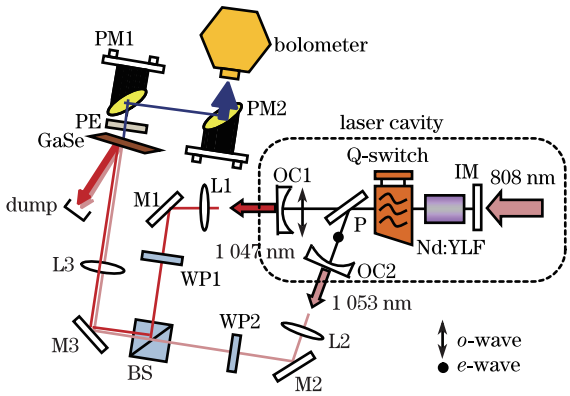

Fig. 9. Experimental setup for the THz DFG based on the compact and portable dual-frequency Nd:YLF laser having dual cavities: laser input mirror (IM); polarizer (P); laser output couplers (OC1-OC2); convex lenses (L1-L3); high reflection mirrors (M1-M3); half-wave plates (WP1-WP2); high-density white polyethene filter (PE); and parabolic mirrors (PM1-PM2).

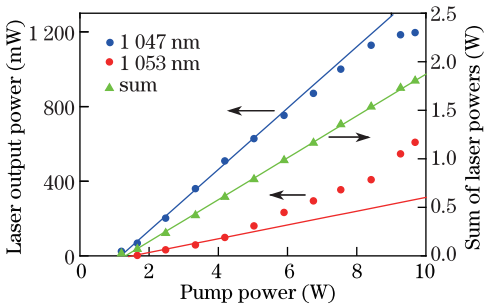

Fig. 10. Dependence of powers from the dual-frequency Q-switched Nd:YLF laser on the pump power from the laser diode.

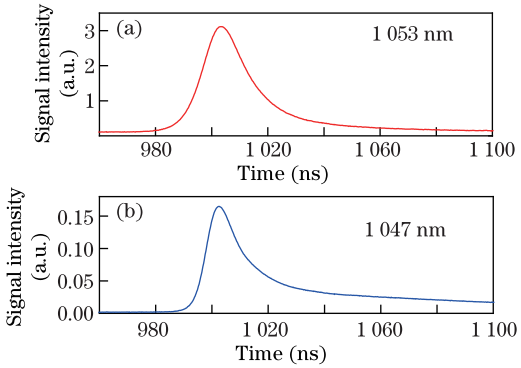

Fig. 11. Temporal profiles of dual-frequency output pulses generated by the Q-switched Nd:YLF laser. (a) 1 053 nm and (b) 1 047 nm.

shows that below the pump power of 5 W, both output powers increase linearly with the pump power. In addition, the powers at 1 047 nm are significantly higher. Higher than 5 W, however, the output power at 1 047 nm is slightly saturated, whereas the output power at 1 047 nm increases at a higher rate. This can be accounted by the two transitions accessing the same population of electrons in the upper lasing level. When the gain for one transition was saturated, the gain for the second one increased. Therefore, the dependence for the sum of the output powers remained linear, which agrees well with the theory for the solid-state laser[38]. By measuring the output powers as a function of the repetition rate, we found an optimal repetition rate of 3.9 kHz for the Q-switch in terms of the THz output powers. At the pump power of 9.69 W, the output powers of 1.196 W and 0.608 W at 1 047 nm and 1 053 nm, respectively, were generated corresponding to the net conversion efficiency of 18.6%. The ratio of the output powers at the two wavelengths is approximately 2:1. By further optimizing the design of the optical cavities, we can reduce the ratio to nearly 1:1. At the pump power of 5.9 W, M^2 factors are 5.18 and 3.07 for 1 047 nm and 1 053 nm, respectively. The poorer beam quality at 1 047 nm is attributed to the tilting of its cavity mirror, which was used to reduce the ratio of the output powers for the two transitions. The pulse shapes of the two output beams are shown in Fig. 11. The two pulse trains were measured simultaneously using two photodiodes. According to Fig. 11, the two pulses were synchronized. At the pump power of 9.69 W, the pulse widths are 15.47 ns and 18.59 ns at 1 047 nm and 1 053 nm, respectively.

Using two convex lenses with the same focal length, the two beams were collimated and combined by a polarization cube, as shown in Fig. 9. The polarization cube was adjusted in such a way that the optical paths at the two wavelengths are exactly the same. As a result, the two input beams were overlapped in both time and space and focused on the 15-cm-long GaSe crystal using a convex lens (L3). After the DFG, the residual pump beams were blocked using a white polyethylene filter. The reflected pump beams were collected by a beam dump. The generated THz beam was collected by two off-axis parabolic mirrors and focused onto a power meter. The input beams at 1 047 nm and 1 053 nm are the ordinary and extraordinary waves inside the crystal whereas the THz wave is an extraordinary wave. The external phase-matching angle was measured to be 11.5°, which is close to the theoretical value of 11°[33]. The azimuthal angle has been optimized in our experiment to reach the optimal value of the effective nonlinear coefficient[33]. The output wavelength was measured by scanning an Si-based etalon, based on the Fig. 12 inset. The output wavelength was measured to be 183.3 μm, which agrees well with 182.4 μm which has been calculated from the two input wavelengths of 1.046 66 μm and 1.0527 μm[38]. The dependence of the average and peak output powers were plotted on the sum of the output powers generated by the Nd:YLF laser as the input powers for the DFG (Fig. 12). The solid curve corresponds to the quadratic fit of the data points, which is consistent with the characteristics of the DFG. Based on the experimental result, the average output power reached the optimal values at the repetition rate of 3.9 kHz. When the sum of the input powers was 1.8 W, the average output power from the GaSe crystal was measured to be 0.948 μW. The pulse width for the THz beam was deduced to be 12.36 ns by measuring the temporal profile of the sum-frequency signal in a KTP crystal. Based on the pulse width, the highest THz peak power was determined to be 19.7 mW. The linewidth of the THz wave was estimated to be 65 GHz by measuring the linewidth of the sum-frequency signal (i.e., 0.06 nm). A DLATGS pyroelectric detector operating at room temperature can have a noise equivalent power of as low as 230 pW. Therefore, the output power of 0.948 μW corresponds to a dynamic range of 4120, which is sufficiently high for realizing the key applications mentioned in section 1. We can further improve the output powers to at least 100 μW by placing a nonlinear crystal inside the optimized Nd:YLF laser cavities.

5. Power scalability and frequency agility

In this section, the results of the introduction of the two laser crystals to generate two different output frequencies[30] are summarized. The experimental result illustrates that the output powers of the solid-state lasers based on the two crystals significantly improved. Consequently, the THz output power was improved by mixing the two laser frequencies in a nonlinear crystal. After the second laser crystal was introduced, the compactness of THz source was maintained. Moreover, this configuration can be used to extend to the combinations of different laser crystals to generate different output

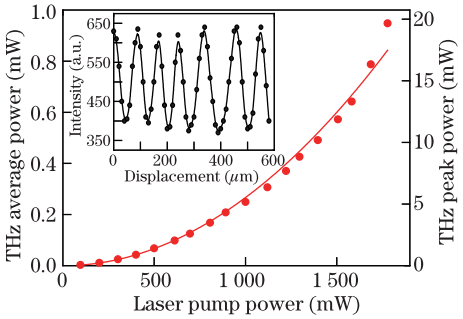

Fig. 12. Dependencies of the average and peak output powers on the sum of the output powers generated by the single Nd:YLF laser. The solid curve corresponds to the quadratic fit to the data points. Inset: the plot of power being transmitted through a Si etalon versus the distance between the two Si plates in the etalon.

frequencies.

The experimental setup for the new configuration of laser cavities is shown in Fig. 13. The input mirror 1, polarizer, and output coupler compose the first cavity for lasing at 1 053 nm whereas the input mirror 2, polarizer, and output coupler make up the second cavity for lasing at 1 047 nm. This cavity configuration is completely different from the cavity configuration in the previous section[29], where the Nd:YLF crystal was placed at the arm and shared by the 1 047 nm and 1 053 nm cavities. In deed, in section 4, the two radiation beams at 1 047 nm and 1 053 nm accessed the same population inversion within a single Nd:YLF crystal pumped by the same diode laser. Given that the 1 047 nm and 1 053 nm beams have perpendicular polarization directions, an intracavity polarizer was introduced to separate the two beams from the two cavities. This approach alleviated the gain competition between the 1 047 nm and 1 053 nm radiation beams inside the Nd:YLF crystal. However, due to the competition, we observed the unbalanced powers between the two frequencies, as described in the previous section[29]. In our current configuration, two Nd:YLF crystals (a-cut, Nd doped at 1.0%, and 4×4×10 (mm)) were introduced and labeled as laser crystals 1 and 2 in Fig. 13. The two laser crystals were placed at the two divided arms decoupled by the polarizer. As a result, the 1 047-nm and 1 053-nm transition beams managed to access the population inversions from two separate gain media, representing an ultimate solution to the gain competition. An acoustic-optic Q-switch was placed at the shared arm of the two laser cavities. Thus, the dual-frequency pulses are synchronized by simultaneously modulating the losses of the two cavities. The other improvement of the cavities is an output coupler shared by the two cavities, i.e., a concave mirror (curvature=15 cm) having a reflectivity of R=75% at both 1 047 nm and 1 053 nm. Because the dual-frequency beams are emitted from the same output coupler (Fig. 13), the two beams are collinearly propagating. To generate a THz output based on frequency-mixing, a nonlinear crystal can be placed right after the output coupler. Therefore, the THz source can become truly compact.

The two diode pump beams at 808 nm were collimated and focused onto the Nd:YLF crystals through a couple of convex lenses, respectively. The diode pump power can be tuned separately. This feature is quite critical for synchronizing the dual-frequency pulses when the lasers are operated at the pulsed mode. In this case, the pulse build-up times for the two lasers must be exactly the same. When the acoustic-optic become highly transparent, the laser pulse is not generated instantly. The pulse build-up time is the time it takes to generate the laser pulse when the Q-switch is instantly opened. This value is determined by the stimulated emission cross section of the laser gain medium, loss of the cavity, output coupling coefficient, and pumping level above threshold. Once the laser crystals are chosen and the cavity is well aligned, the former three factors cannot be changed. As a result, the only way for changing the pulse build-up time is through the pump power level. In our configuration, the pump power levels of the two lasers can be changed independently by simply varying the driving currents of the lasers.

When the repetition rate of the Q-switch is set at 5 kHz, the dependence of the Q-switched output powers on the pump powers at both 1 047 nm and 1 053 nm (Fig. 14) can be measured. Both the output powers at 1 047 nm and 1 053 nm increased linearly. As a result, the issue of gain competition in the previous section is completely addressed[29]. The output powers of 2.8 W and 1.918 W at 1 047 nm and 1 053 nm were obtained at pump powers of 10.55 W and 9.55 W, corresponding to the net conversion efficiencies of 26.5% and 20.1%, respectively. The corresponding slope efficiencies are 29.8% and 22.5%, respectively. Compared with the results in the previous section[29], the total output power has been improved by more than twice. In addition, the ratio of the slope efficiencies between 1 047 nm and 1 053 nm is 1.32, which is close to the ratio of the corresponding stimulated cross sections (i.e., 1.5)[29].

A 15-mm-long GaSe crystal was used to measure the THz output by mixing the two laser beams (Fig. 13). The GaSe crystal was placed directly after the output coupler. This setup is different from the previous one where a beam splitter was used to combine the two dual-frequency beams onto a nonlinear crystal. Obviously, the configuration illustrated in Fig. 13 is more compact. The power dependence was measured (Fig. 15). At the highest incident power of 4.24 W, an output power of 4.464 μW at 1.643 THz (182.4 μm) was achieved. Figure 15 shows that the dependence is nearly quadratic, which is a characteristic for the DFG. Compared with the previous result, the output power increased by 4.7. This enhancement is attributed to the improvement of the laser powers at 1 047 nm and 1 053

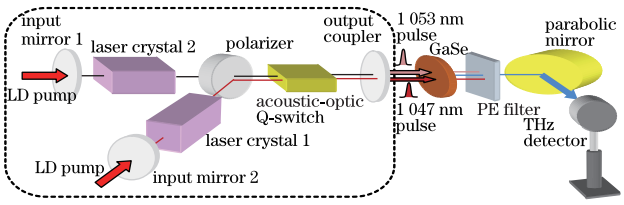

Fig. 13. Experimental layout for a configuration of the dual-frequency solid-state laser and compact THz source. The dual-frequency laser cavities are marked by the dashed border lines.

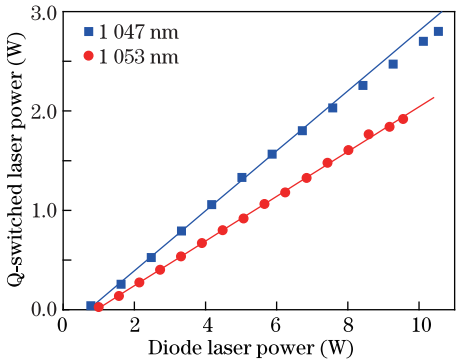

Fig. 14. Q-switched output power versus the pump power at 1 047 nm and 1 053 nm. The dots and squares correspond to the data points. The straight lines correspond to the linear fits to the data points.

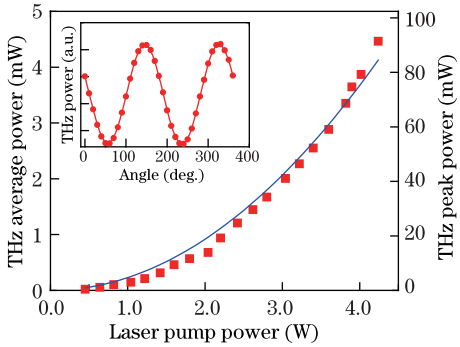

Fig. 15. THz average and the peak power dependence on the combined power at 1 047 nm and 1 053 nm; the solid curve corresponds to the quadratic fit to the data points. Inset is the intensity of the THz radiation as a function of the azimuthal angle of a THz polarizer. The solid curve in inset corresponds to the nonlinear least squares fit to the data points.

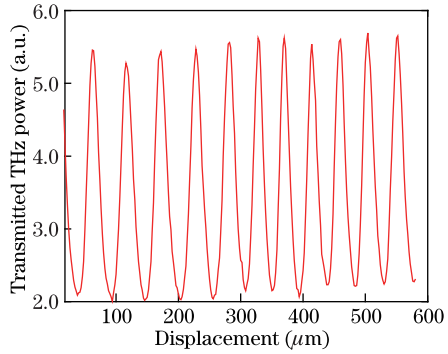

Fig. 16. THz power at 100.5 μm, generated by mixing dual frequencies from the Nd:YLF and Nd:YAG lasers being transmitted through a Si etalon as a function of the displacement between two Si wafers.

nm. The pulse widths at 1 047 nm and 1 053 nm are 17.7 ns and 11.71 ns, respectively. The laser linewidths are 77.5 GHz and 76.5 GHz, respectively. Assuming that the pulse shape is Gaussian, the pulse width of THz radiation is estimated to be 9.766 ns. The polarization of the THz radiation was also measured as a function of the azimuthal angle of a THz polarizer, as shown by the inset of Fig. 15. Based on the sinusoidal oscillation, the THz polarization can be determined.

One of the advantages of our configuration is the ability to generate the THz output frequency simply by choosing two different laser crystals. Considering that more than 100 Nd-doped laser materials or ceramics have been studied[39] whose wavelengths cover the range of 1.03 to 1.1 μm, it is conceivable for us to generate any THz output wavelength. To demonstrate the frequency agility, the Nd:YLF crystal was replaced with a 10-mm-long and 1.0% Nd-doped YAG crystal. The rest of the optical components used were the same. At the diode pump powers of 9.55 W and 8.653 W, the output powers of 1.981 W and 1.706 W at 1 053 nm and 1 064 nm, respectively were generated. At the repetition rate of 5 kHz, the pulse widths are 9.92 ns and 12.48 ns, respectively. The laser linewidths are 76.5 GHz and 75.0 GHz, respectively. By mixing the two laser beams on the GaSe crystal, we generated the THz radiation at 2.983 THz (100.5 μm). The external phase-matching angle for the type II DFG is 18.3°, which is consistent with the theoretical value[33]. The highest output power is 2.09 μW. The lower output power at such frequency, compared with the output power at 1.64 THz, is due to the increased absorption of the THz radiation by the GaSe crystal. The estimated THz pulse width is 7.766 ns. The THz output wavelength was measured by scanning a Si-based etalon (Fig. 16). Figure 16 shows that the output wavelength is 98 μm, which is close to 100.5 μm, calculated from the two pump wavelengths. The THz linewidth is deduced to be 42 GHz (Fig. 16). This value is close to 53.5 GHz, which has been estimated from the laser linewidths. Using surface-emitting geometry[40,41], it is feasible to extend the output wavelengths to the far-infrared region.

6. Conclusion

We have reviewed the recent results on the THz generation based on DFG. In particular, we demonstrate that using only four reversely stacked GaP plates, maximum conversion efficiency of 40% in terms of photon numbers can be achieved. By adding the fifth GaP plate to the stack, the THz output power is significantly reduced compared with that of the four stacked plates. This is the evidence of the occurrence of back conversion. On the other hand, to make the THz source truly compact and portable, a completely different approach to the THz source is implemented. By mixing the two frequencies generated by a dual-frequency Nd:YLF laser a compact and portable THz source with an average output power reaching 1 μW is obtained. By introducing two Nd:YLF crystals, instead of one inside the laser cavity, the output power is significantly scaled up to 4.5 μW. Through further optimizations and use of novel configurations, the THz output power can be improved to the mW level. The dimensions of the THz source used in the experiment are approximately 12×12×6 (inch), which can be readily reduced to 12×6×4 (inch) through further optimizations. Our future goal is to develop a THz source which is as compact as a laser pointer, which will be operated at room temperature.

We are indebted to Y. Jiang for the valuable contributions to some of the projects reviewed in this article.

This work has been supported by the U.S. National Science Foundation.

References

1. W. Gordy and R. L. Cook, *Microwave Molecular Spectra* (Jchn Wiley & Sons, New York, 1984).
2. R. A. McClatchey, R. W. Fenn, J. E. A. Selby, F. E. Volz, and J. S. Garing, in *Handbook of Optics*, W. G. Driscoll (eds.), (McGraw Hill, New York, 1978).
3. A. Bykhovski, T. Globus, T. Khromova, B. Gelmont, and D. Woolard, Int. J. High Speed Electron. Syst. **17,** 225 (2007).
4. A. Lee, Q. Qin, S. Kumar, B. S. Williams, Q. Hu, and J. L. Reno, Appl. Phys. Lett. **89,** 141125 (2006).
5. L. Xu, X.-C. Zhang, and D. H. Auston, Appl. Phys. Lett. **61,** 1784 (1992).
6. D. H. Auston, K. P. Cheung, and P. R. Smith, Appl. Phys. Lett. **45,** 284 (1984).
7. D. H. Auston, K. P. Cheung, J. A. Valdmanis, and D. A. Kleinman, Phys. Rev. Lett. **53,** 1555 (1984).
8. K. P. Cheung and D. H. Auston, Infrared Phys. **26,** 23 (1986).
9. M. van Exter, C. Fattinger, and D. Grischkowsky, Opt. Lett. **14,** 1128 (1989).
10. H.-B. Liu, Y. Chen, G. J. Bastiaans, and X.-C. Zhang, Opt. Exp. **14,** 415 (2006).
11. D. M. Mittleman, S. Hunnsche, L. Boivin, and M. C. Nuss, Opt. Lett. **22,** 904 (1997).
12. K. Kawase, M. Sato, T. Taniuchi, and H. Ito, Appl. Phys. Lett. **68,** 2483 (1996).
13. W. Shi, Y. J. Ding, N. Fernelius, and K. L. Vodopyanov, Opt. Lett. **27,** 1454 (2002).
14. W. Shi and Y. J. Ding, Appl. Phys. Lett. **84,** 1635 (2004).
15. W. Shi and Y. J. Ding, Int. J. High Speed Electron. Syst. **16,** 589 (2006).
16. W. Shi and Y. J. Ding, Optics and Photonics New 57 (2002).
17. W. Shi and Y. J. Ding, Appl. Phys. Lett. **83,** 848 (2003).
18. W. Shi, Y. J. Ding, and P. G. Schunemann, Opt. Commun. **233,** 183 (2004).
19. W. Shi and Y. J. Ding, Opt. Lett. **30,** 1030 (2005).
20. Y. J. Ding and W. Shi, Sol. State Electron. **50,** 1128 (2006).
21. W. Shi, X. Mu, Y. J. Ding, and N. Fernelius, Appl. Phys. Lett. **80,** 3889 (2002).
22. W. Shi and Y. J. Ding, Laser Phys. Lett. **1,** 560 (2004).
23. H. Sun, Y. J. Ding, and I. B. Zotova, IEEE Sens. J. **10,** 621 (2010).
24. H. Sun, Y. J. Ding, and Y. B. Zotova, Appl. Opt. **46,** 3976 (2007).
25. R. Song, Y. J. Ding, and Y. B. Zotova, Intern. J. High Speed Electron. Syst. **17,** 251 (2007).
26. R. Song, Y. J. Ding, and I. B. Zotova, Proc SPIE **6949,** 694903 (2008).
27. Y. Jiang, Y. J. Ding, and I. B. Zotova, Appl. Phys. Lett. **96,** 031101 (2010).
28. Y. Jiang, D. Li, Y. J. Ding, and I. B. Zotova, Opt. Lett. **36,** 1608 (2011).
29. P. Zhao, S. R. Ragam, Y. J. Ding, and I. B. Zotova, Opt. Lett. **35,** 3979 (2010).
30. P. Zhao, S. Ragam, Y. J. Ding, and I. B. Zotova, Appl. Phys. Lett. **98,** 131106 (2011).
31. L. P. Gonzalez, S. Guha, and S. Trivedi, in *Proceedings of CLEO Technical Digest on CD-ROM CWA47* (2004).
32. F. L. Madarasz, J. O. Dimmock, N. Dietz, and J. Bachmann, J. Appl. Phys. **87,** 1564 (2000).
33. D. N. Nikogosyan, *Nonlinear Optical Crystals* (Springer, New York, 2005).
34. A. Yariv, *Quantum Electronics* (John Wiley & Sons, New York, 1989) p. 399.
35. B. Frei and J. E. Balmer, Appl. Opt. **33,** 6942 (1994).
36. H. Zbinden and J. E. Balmer, Opt. Lett. **15,** 1014 (1990).
37. B. Wu, P. Jiang, D. Yang, T. Chen, J. Kong, and Y. Shen, Opt. Express **17,** 6004 (2009).
38. W. Koechner and M. Bass, *Solid-State Lasers* (Springer, New York, 2003) pp. 63-65.
39. F. Trager (eds.), *Handbook of Lasers and Optics* (Springer, New York, 2007).
40. Y. Avetisyan, Y. Sasaki, and H. Ito, Appl. Phys. B **73,** 511 (2001).
41. Y. J. Ding, Opt. Lett. **35,** 262 (2010).